Article:
Keane, RJ, Parker, DJ and Fletcher, JK (2021) Biases in Indian summer monsoon precipitation forecasts in the Unified Model and their relationship with BSISO index. Geophysical Research Letters. ISSN: 0094-8276

https://doi.org/10.1029/2020gl090529

Biases in Indian summer monsoon precipitation forecasts in the Unified Model and their relationship with BSISO index.

R. J. Keane[1,2], D. J. Parker[2], J. K. Fletcher[2]

[1]Met Office, FitzRoy Road, Exeter EX1 3PB, UK
[2]School of Earth and Environment, University of Leeds, Leeds LS2 9JT, UK

Key Points:

- The low-precipitation bias in the Indian Summer Monsoon is dominated by break and break-to-active transition periods.
- There is evidence that the bias is strongly linked to an inability to simulate low-pressure systems.
- A reduction in the incoming moisture flux from the Arabian Sea also occurs from about 3 days for all modes of intraseasonal variability.

Corresponding author: Richard Keane, `richard.keane@metoffice.gov.uk`

Abstract

This study shows that the Boreal Summer Intraseasonal Oscillation (BSISO) dominates the Indian summer monsoon low-precipitation bias in the Met Office Unified model. Analyzing a recent 9-year period (June, July, August only), it is found that the precipitation bias is dominated by break and break-to-active transition BSISO phases, while some of the other phases have no bias at all over a 7-day forecast. Evidence of a link to upstream effects is found, in that there is a delayed reduction in the moisture flux entering India from the west. It is also shown that an increase in the net flow of moisture out of India to the east is strongly linked to the low-precipitation bias, and there is some evidence that this is related to a lack of low-pressure systems over India. Most atmospheric models have substantial rainfall biases over India, and these results may indicate the circulation patterns responsible.

Plain Language Summary

The Met Office Unified Model (UM) is widely used worldwide for weather forecasting, climate prediction and environmental research. An important deficiency of the UM, in common with many other weather and climate models, is that it simulates significantly too little rainfall over India, when averaged over the summer monsoon season. Indian monsoon rainfall is important to the livelihoods of hundreds of millions of people, and these errors in the models have knock-on consequences for weather and climate prediction around the world. This study shows that the UMs rainfall bias is dominated by periods when the general monsoon behavior is in transition from low-activity to high-activity, while in other periods, the rainfall forecasts perform much better. These results will help us to better understand the causes of the model bias. A systematic evaluation of the UM moisture flow has also been carried out; this suggests that a key problem in these low to high-activity transition periods is a replacement of monsoon cyclonic systems with too much purely westerly flow out of India. The results should also be of value in weather forecasting, in identifying weather regimes where we have relatively high, and relatively low, confidence in the forecasts.

1 Introduction

The lack of sufficient precipitation over India during the Indian Summer Monsoon (ISM) is one of the most significant and persistent biases in the Met Office Unified Model (UM) (Walters et al., 2017; Williams et al., 2018; Keane et al., 2019), a General Circulation Model used at operational centers and research institutions worldwide (Brown et al., 2012; Bi et al., 2013; Bermous & Steinle, 2015; Noh et al., 2016; Kar et al., 2019; Walters et al., 2019, for example). As well as its considerable soicioeconomic importance, the ISM is one of the most challenging atmospheric phenomena to simulate, and is therefore of great dynamical interest. Although interannual variability in all-India rainfall is only about 10%, sub-seasonal active and break periods significantly affect agriculture and industry (Krishnamurthy & Shukla, 2000). These active and break cycles can be characterised in numerous ways. Here we use the Boreal Summer Intraseasonal Oscillation (BSISO) (Zhu & Wang, 1993; Wang & Xie, 1997; Webster et al., 1998) to characterise active and break spells in the ISM. The BSISO is in many ways the boreal summer analogue to the MJO, but it is differentiated from the latter in its northwest to southeast tilt and its northeastward propagation, rather than purely eastward propagation. The BSISO strongly influences Indian rainfall on 20–60 day timescales.

Substantial progress has been made in understanding the causes and nature of the bias in seasonal and climate simulations: it has been related to a high-precipitation bias over the Indian ocean (Bush et al., 2015), an inability to correctly simulate low pressure systems in the region (Levine & Martin, 2018), poor representation of deep convection (Willetts et al., 2017), a southward shift of the Intertropical Convergence Zone (Haywood

et al., 2016, ITCZ) and an anticyclonic bias (Martin & Levine, 2012; Levine & Martin, 2018). However, the low-precipitation bias remains in the most recent version of the UM (Walters et al., 2019). There are also many other widely used models with similar biases (Sperber et al., 2013; Almazroui et al., 2020; Pathak et al., 2019; Wang et al., 2020; Gusain et al., 2020), so understanding the bias in the UM could have wider implications for atmospheric modeling more generally.

Keane et al. (2019) recently demonstrated that some of the findings mentioned above, on understanding the low-precipitation bias in the UM, also apply on shorter time scales, by investigating moisture budgets in operational weather forecasts. They identified that the dry bias is associated with (i) a reduction in moisture-carrying flow from the Arabian Sea, which only appears approximately three days into the forecast, suggestive of upstream effects over the Indian Ocean, and (ii) an anticyclonic bias over north-eastern India, which moves within this region throughout the forecast. A drying of the air itself flowing into India was also identified, including both moist air from the Arabian Sea and already dry air from the land to the northwest; this drying occurred from very early in the forecast. Kar et al. (2019) also found a reduction in precipitation for shorter-range UM forecasts during the ISM, accompanied by an anticyclonic bias.

The present study extends the work of Keane et al. (2019) to cover operational forecasts for June–August (JJA) of all the years 2011–2019. Using this extended period, it is possible to divide the dataset into categories, here defined by the BSISO index, and to investigate how the low-precipitation bias varies with category.

2 Data and Methods

2.1 Operational forecasts

Global NWP forecasts were taken from the Met Office operational archive, valid within JJA 2011–2019. During this period the forecasts were initialized four times per day, and fields were here retrieved at lead times every 12 hours starting at 0 hours and ending at the end of the forecast (here 168 hours for forecasts starting at 0000 and 1200 UTC and 60 hours for forecasts starting at 0600 and 1800 UTC). Only forecasts with valid times occurring inside the JJA period (0000 UTC on 1st June to 1800 UTC on 31st August inclusive) were included, so that forecasts initialized towards the end of May were partially included and forecasts initialized towards the end of August were partly excluded. For the precipitation accumulations, only forecasts starting at 0000 and 1200 UTC were used.

Two versions of the UM, at three different resolutions, were used during the period studied, with an upgrade from GA3.1 to GA6.1 in July 2014 (Table S1 provides details). The output fields used in this study are 12-hour accumulated precipitation, instantaneous values of pressure, specific humidity, eastward wind, northward wind (all four on model levels), precipitation, upward surface moisture flux and 6-hour or 3-hour (depending on year) mean surface latent heat flux.

2.2 Moisture budget analysis

The moisture budget analysis is described in detail in Keane et al. (2019). It is based on evaluating the net moisture flux into a region bounded between two latitudes, here 8°N and 29°N, and two longitudes, here 69°E and 89°E (making a region somewhat larger than that studied in Keane et al. (2019); the precise boundaries are given in Table S1). The rate of change of moisture into the region is given by:

$$\mathbb{Q}_t = \mathbb{M}_\mathrm{W} + \mathbb{M}_\mathrm{E} + \mathbb{M}_\mathrm{S} + \mathbb{M}_\mathrm{N} + \mathbb{E} - \mathbb{P}. \quad (1)$$

Here $\mathbb{M}_\mathrm{W}$, $\mathbb{M}_\mathrm{E}$, $\mathbb{M}_\mathrm{S}$ and $\mathbb{M}_\mathrm{N}$ are the horizontal moisture flux into the region on the western, eastern, southern and northern sides, respectively, integrated over the length of the side and the full height of the column. $\mathbb{E}$ and $\mathbb{P}$ are horizontal area integrals over the whole region of, respectively, surface upward water flux and precipitation. A further quantity

$$\mathbb{M}_\mathrm{A} = \mathbb{M}_\mathrm{W} + \mathbb{M}_\mathrm{E} + \mathbb{M}_\mathrm{S} + \mathbb{M}_\mathrm{N} + \mathbb{E} \tag{2}$$

is defined as the total net moisture flux 'available' for precipitation in the region. Each quantity is given in kg/s and, as in Keane et al. (2019), is divided by the total area of the region (which varies slightly as shown in Table S1), to give a value in $\mathrm{kg\,m^{-2}\,hr^{-1}}$, which is expressed here as mm/hr.

Each of the terms in Eq. 1 is evaluated for each forecast lead time and each valid time (so that, for a given valid time, the quantities for each lead time will have come from a different forecast). For each year, the evaluation period is divided into 184 12-hour sections, with each section containing a 168-hour forecast starting at 0000 or 0012 UTC and a 60-hour forecast starting at 0600 or 1800 UTC. For lead times up to 60 hours, the quantity taken is the average of the forecast pair at that lead time. After 60 hours, the 0000 or 0012 UTC forecast at that lead time is used, but it is calibrated to estimate what the average of the forecast pair would have been, if an 0600 or 1800 UTC forecast had also been available. This is done by assuming a constant offset between each pair of forecasts, and estimating this based on the average difference of all 184 pairs of forecasts, over all lead times up to 60 hours. The upward surface moisture flux is not available at all after 60 hours so this is estimated using the surface latent heat flux. The calibration process is described in detail in the Appendix of Keane et al. (2019).

2.3 BSISO index

In order to categorise the data by BSISO state, we use the bimodal ISO index of Kikuchi et al. (2012). This index is calculated using extended empirical orthogonal function analysis on 25–90-day filtered daily NOAA outgoing longwave radiation data and has both an MJO mode (for boreal winter) and a BSISO mode (for boreal summer). The BSISO index is defined with a phase and amplitude analogous to that of Wheeler and Hendon (2004). The daily phase and amplitude data were accessed at `http://iprc.soest.hawaii.edu/users/kazuyosh/ISO_index/data/BSISO_25-90bpfil.rt_pc.txt` in October 2019. For each 12-hour period in the UM data, quantities are allocated the phase corresponding to that day, unless the amplitude for that day is less than 1, when it is allocated phase 0 (so there are always two consecutive 12-hour sections with the same phase).

In this study, forecasts are categorised according to the BSISO phase at the forecast valid time. Longer forecasts will therefore have passed through one or two other BSISO phases before reaching the valid time: the typical BSISO period is about 39 days so that, with 8 phases, a forecast changes phase approximately every 4.9 days on average. Quantities relating to each BSISO phase are calculated by averaging over all 12-hour periods that have been allocated that phase, over the nine 3-month periods.

3 Results

3.1 Precipitation accumulation

Keane et al. (2019) showed that Indian summer monsoon (ISM) precipitation decreases with forecast lead time in the Met Office operational NWP forecast, for each year 2012–2017, although the initial bias with respect to observations varied. Figure S1 extends this to 2011–2019 and shows that the reduction in precipitation with forecast lead time is widespread within the study region for all years. The climate bias against GPCP

observations (Adler et al., 2003) is also shown for comparison; it is conceivable that the reduction in precipitation over 7 days of NWP forecast is relevant to why the climate simulation produces too little precipitation over a much longer period. The situation is somewhat complicated by the fact that the NWP forecast at the shortest lead times actually has a positive bias against observations (see below) but, despite this, by day 7 the NWP forecast already has a negative bias against observations (see below and Figure S2).

Figure 1 shows the precipitation accumulation, averaged over the inside of the green box shown in Figures S1, 3, 4 and S6 (and defined in subsection 2.2), as a function of BSISO phase, at the start of the forecast, at the end of the forecast and in observations from IMERG (Huffman et al., 2019) and GSMaP (Kubota et al., 2020). From this, we define the phases as follows: 4–6 as 'active' phases; 8, 1 and 2 as 'break' phases; 2–4 as break→active transition phases; and 6–8 as active→break transition phases (so that the even phases are each defined in two categories: for example, phase 2 is a break phase but starting to transition to active). Active/break periods are thus defined according to a dynamical driver of precipitation, rather than actual values of precipitation during each period. The accumulation at the start of the forecast is clearly too high, which is indicative of issues with the convection parameterization on short time scales, although it does follow broadly the same distribution as the observed precipitation.

The precipitation at the end of the forecast is lower than that at the start of the forecast for all phases, indicating that a reduction in precipitation does occur through all phases. However, the reduction varies substantially with phase, to the extent that, for phases 5–8, the final accumulation is still higher than or close to the observed precipitation. For these phases, it is not clear whether or not there is a low-precipitation bias at all: if the forecast were continued for longer, then the precipitation could plausibly either remain close to the observed value, or continue to decrease so that after a longer time it was substantially below the observed value. This behavior of initial precipitation being higher than observed, but reducing systematically in NWP forecasts, was also demonstrated by Kar et al. (2019), and has been shown to occur over a recent 9-year period by (Sharma et al., 2019) (their Figure 4).

For phases 1–4, meanwhile, there is clearly a low-precipitation bias by the end of the forecast, with respect both to observations and to the values at the start of the forecast. These phases account for most of the low-precipitation bias with respect to observations, and for a substantial part of that with respect to the start of the forecast. Since local processes are particularly important during these phases, it is possible that the reduction in precipitation is partly caused by the atmosphere drying out excessively at the start of the forecast due to the high-precipitation bias. It is plausible that this decrease in precipitation would continue in a longer forecast, and could potentially be linked to the low-precipitation bias seen in climate simulations, although further work on seasonal UM forecasts would be required to establish this connection.

The transition periods are delayed in the model, so that the bias is worst for break→active transition phases (this could, for example, represent a delayed northward propagation of large-scale rainbands into India) and least bad for active→break transition phases. The greater bias for break→active transitions could be caused by the fact that they are generally more chaotic, associated with fast-growing convective instability, while the active→break transitions are governed by more predictable low-frequency Hadley cell oscillations (Goswami & Xavier, 2003). In general the bias is more negative for break than for active phases, although this is secondary to the effect of the transitions (biases for phases 4–6 are less negative than phases 8, 1 and 2 as a whole, although that for phase 4 alone is more negative).

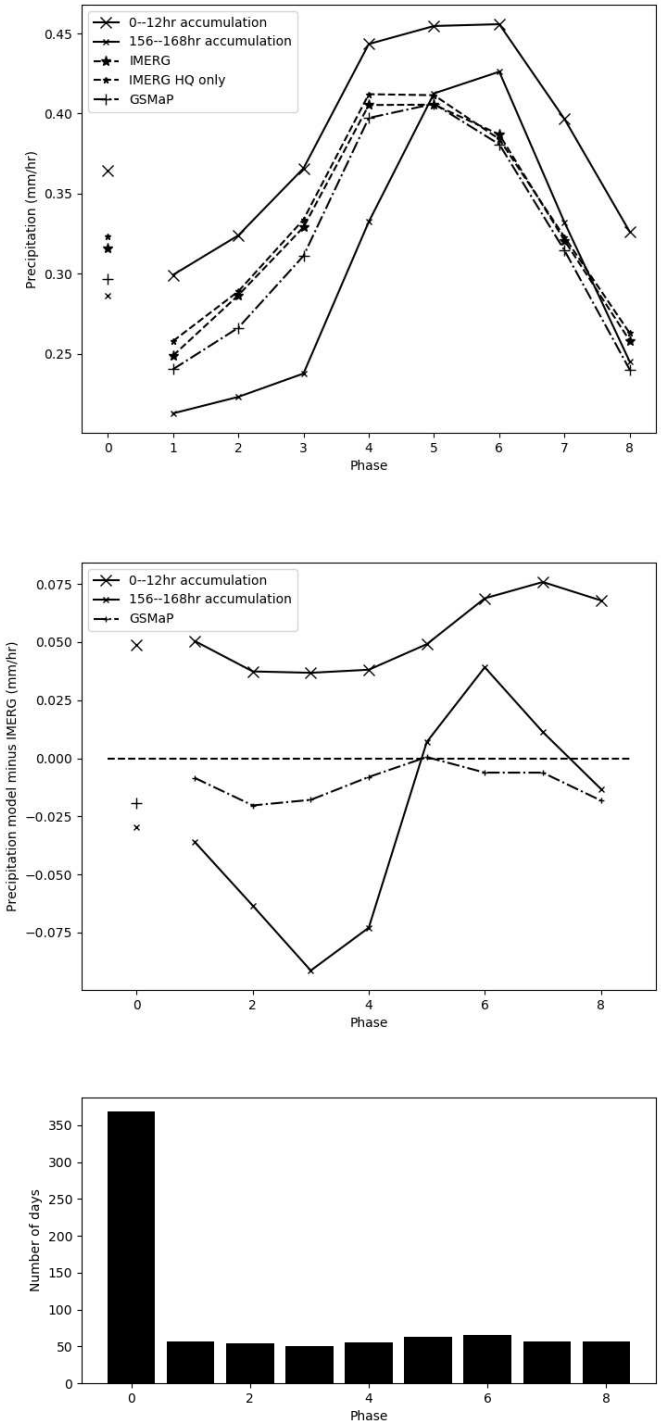

Figure 1. Top panel: Precipitation accumulation as a function of phase for observations, NWP 0–12hr and NWP 156–168hr. The two dashed lines give an idea of the uncertainty in the observations, showing the values with and without the use of infrared observations where microwave observations are not available. Middle panel: As top panel, but showing differences compared with IMERG data. Bottom panel: Distribution of phases across the 9×3-month period.

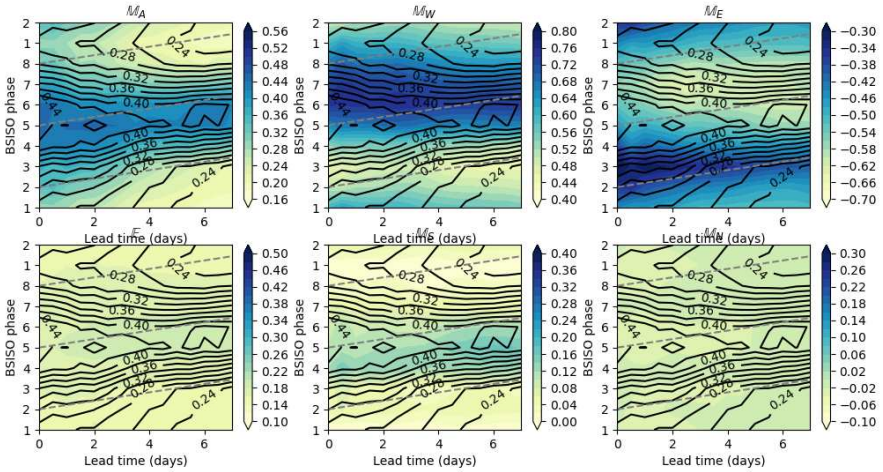

Figure 2. Moisture budget terms as a function of BSISO phase and forecast lead time (phase 0 omitted). Black contours representing precipitation are reproduced in each panel and the colored contours represent other moisture budget terms defined in equations 1 and 2. The dashed grey lines represent the progress of an actual forecast, given a **typical** BSISO period of 39 days.

3.2 Moisture budget terms

Figure 2 shows the variation in moisture budget terms as a function of BSISO phase and forecast lead time. The same information is presented differently in Figures S3 and S4. Although the black contours in Figure 2 (and the black lines in Figures S3 and S4) represent instantaneous, rather than accumulated, precipitation, the similarities with Figure 1 (top panel) are clear. For example, values are generally highest for phases 4–6, and lowest for phases 8, 1 and 2, while the bias between the end and start of the forecast is smallest for phases 5 and 6, and largest for phases 1–3.

Looking at the variation of the terms with phase at day 0, the overall moisture budget is initially well balanced ($\mathbb{M}_A \approx \mathbb{P}$ for all phases) and the variation in $\mathbb{M}_A$ with BSISO phase is driven mainly by variation in $\mathbb{M}_W$, $\mathbb{M}_E$ and $\mathbb{M}_S$. The overall westerly flow is generally weakest (lower values of $\mathbb{M}_W$ and higher, so less negative, values of $\mathbb{M}_E$) during break→active phases, and strongest during active→break phases.

The bias in $\mathbb{P}$ is very similar to that in $\mathbb{M}_A$, with only a slight drying of the region as the forecast develops (in terms of forecast bias, i.e., $\mathbb{M}_A < \mathbb{P}$), mainly for the break phases. The fact that $\mathbb{M}_A$ decreases more quickly than $\mathbb{P}$ is suggestive of biases in horizontal moisture flux causing the bias in precipitation, at least in an overall sense, but further investigation would be required to determine the causality relationship definitively or in detail.

The terms $\mathbb{E}$, $\mathbb{M}_N$ and $\mathbb{M}_S$ are almost constant with lead time and phase, except that $\mathbb{M}_S$ increases substantially from about 4 days for phases 5 and 6. The variation with lead time of $\mathbb{M}_E$ looks very similar to those of $\mathbb{M}_A$ and $\mathbb{P}$, but shifted around two phases earlier, suggesting that an increase in the total moisture flux out of the eastern side of the region is a key driver of the reduction in precipitation. $\mathbb{M}_W$ also clearly reduces from around day 3 for all phases, as was found in Keane et al. (2019), where this delayed reduction was linked to upstream effects over the equatorial Indian Ocean (which may take approximately 3 days to reach the study region).

For phases 6–8, the precipitation recovers somewhat after an early reduction, suggesting that, even for a longer forecast, there may be no low-precipitation bias at all for these phases. It is generally the case that the model performs best when the overall westerly flow is strongest. This could be linked to the fact that there is a tendency for the overall westerly flow to increase near the start of the forecast for all phases.

As mentioned in subsection 2.3, days where the BSISO amplitude is below a threshold of 1 are allocated a phase of 0. In order to determine the effect of this amplitude threshold, Figure 2 is reproduced in Figure S5, but with the allocation to phase 0 removed (so that all days retain their phase 1–8, regardless of amplitude, and the threshold is effectively 0). This looks very similar to Figure 2, but with rather less detail, suggesting that removing the low-amplitude days is effective in enhancing the signal of the variation in phase, without distorting the underlying behavior.

3.3 Spatial variation of moisture fluxes

Figure 3 shows vertically integrated moisture flux (a quantity similar to $\mathbb{M}$, but as a function of space rather than assigned to a specific longitude or latitude line), overlaid on vertically integrated humidity, as a function of horizontal position, for day 0. All phases are characterized by a westerly flow up to 20°N, and cyclonic flow in the north-east of India. Phase 4 is anomalously dry in the north-east of India, coinciding with a much less coherent cylonic flow, but this is outweighed by moist air to the west, making it a wet phase overall. Phases 3 and 4, for which the bias is particularly bad, are both characterized by relatively dry air in north-east India, while phases 5–7, for which the bias is relatively small, are characterized by relatively very moist air over northern India, suggesting that moisture over northern India could be an important factor in the low-precipitation bias.

Figure 4 shows vertically integrated moisture fluxes, overlaid on vertically integrated humidity, as a function of horizontal position, for day 7, and the bias against the analysis. Phases 8, 1, 2 and 3 show a clear drying of the region, in agreement with Figure 2. The other phases show a smaller amount of drying, similar to Figure 2.

For all phases, the cyclonic flow to the north-east of India is weaker by day 7, and the easterlies over the Indo-Gangetic plane have been replaced, to a varying extent, by a purely westerly flow. This effect is more pronounced for the phases where the bias is worst (e.g., 2, 3 and 4). There is a general slight northward shift in the flow into the west side of the region: this seems to account for the increase in flow into the south side of the region for phases 5 and 6 in Figure 2 (there seems to be a slight repositioning of the flux in the southern half of the west side of the box, to the western half of the south side of the box).

The anticyclonic bias seen in Keane et al. (2019) is clearly apparent in this larger dataset. Moreover, it seems to be very important to the low-precipitation bias, as it is clearly worse where the low-precipitation bias is worse. It is certainly reasonable to expect weaker cyclonic flow to lead to lower precipitation, but it is also the case that lower precipitation itself reduces tropospheric heating, leading in turn to weaker low-level circulation. There could, therefore, be a feedback process occurring between the two biases as the forecast develops.

The delayed reduction in flow from the west, seen in Keane et al. (2019) and confirmed in Figure 2 is also apparent in Figure S6, which shows a reduction in westerly flow into the region for all phases, between days 3 and 7. This figure otherwise looks similar to Figure 4, suggesting that the biases seen are not simply due to spin-up or an initial shock from the initial conditions, but may persist in longer UM simulations.

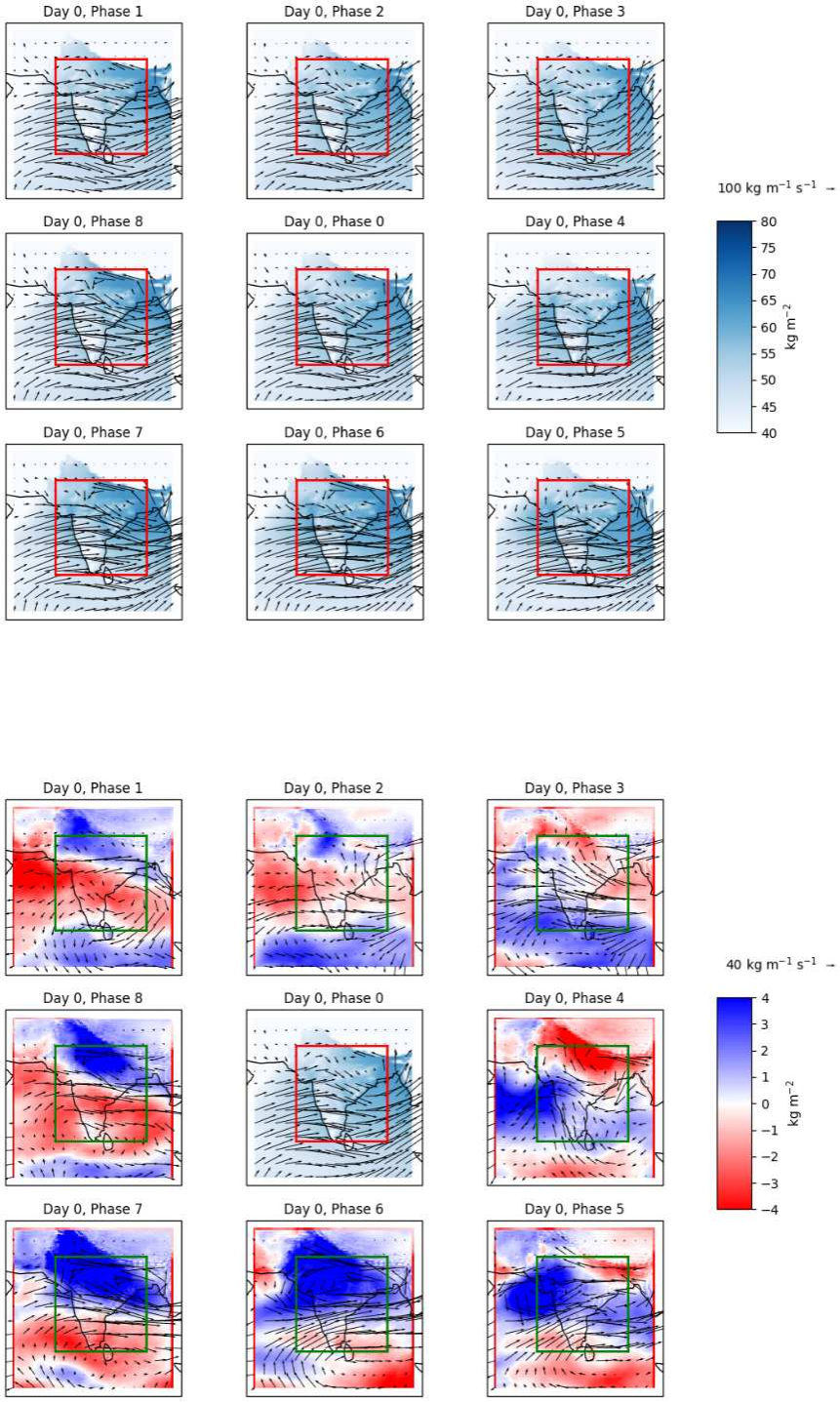

Figure 3. Total column water overlaid with vertically integrated moisture flux vectors. The top panel shows the actual values and the bottom panel reproduces the actual value for phase 0 and shows the anomaly with respect to phase 0 for the other phases (so that the colorbar in the top panel applies to phase 0 in both panels).

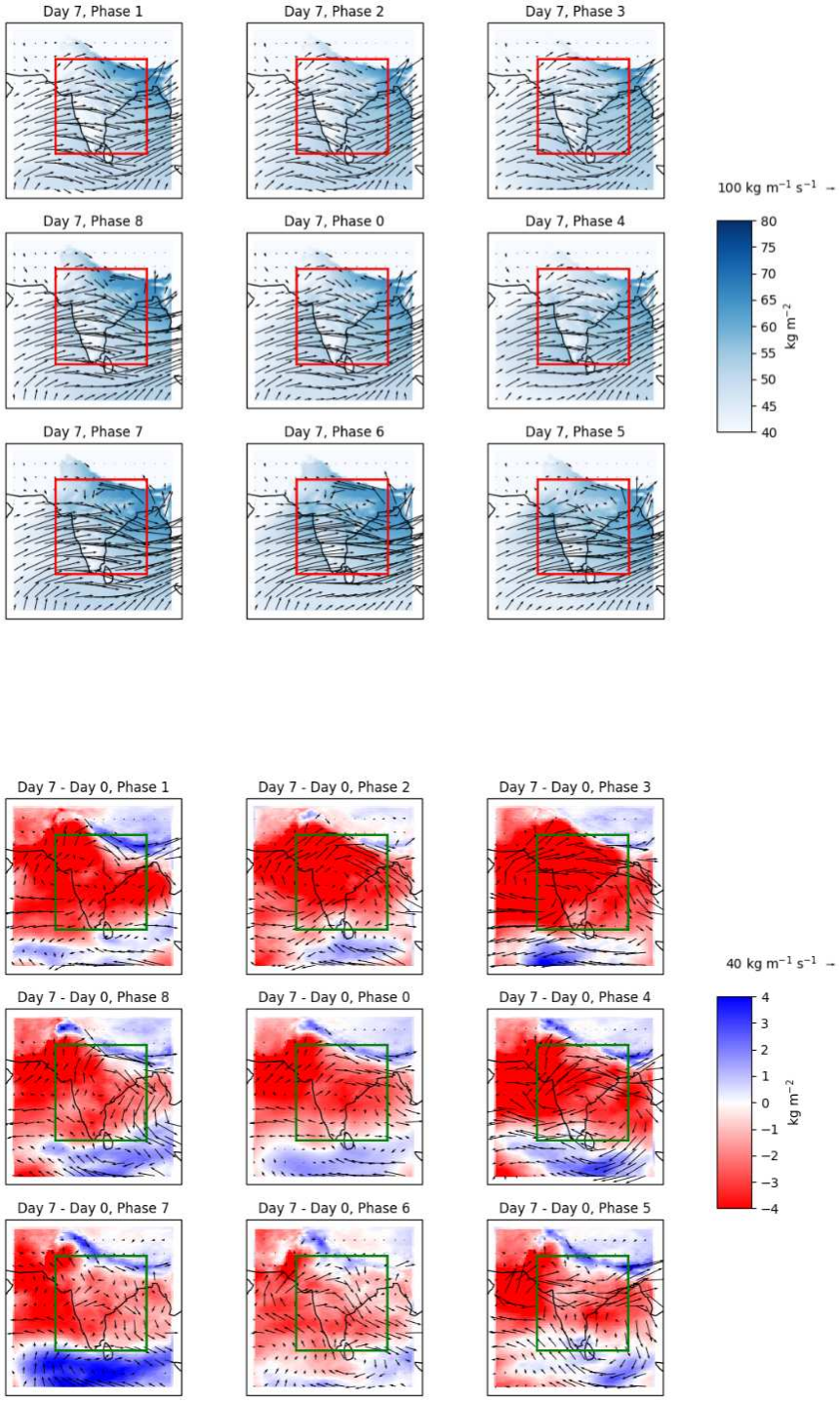

Figure 4. Total column water overlaid with vertically integrated moisture flux vectors for day 7, for each BSISO phase. The top panel shows the actual value and the bottom panel shows the bias against day 0.

4 Conclusions

The well-known low-precipitation bias in the UM for the ISM has been shown to occur for operational weather forecasts during the period 2011–2019. It is found that a substantial part of the bias is accounted for by periods where the BSISO index suggests a break-to-active transition (or, to a lesser extent, a monsoon break). There is some evidence that, when the BSISO index suggests an active-to-break transition, there is no bias at all, although further research (for example looking at seasonal forecasts) will be required to confirm this.

The bias has been shown to be concurrent with an approximately equal bias in the moisture flux entering the region, suggesting that the problem is insufficient moisture entering the region, more than the UM convection scheme reacting incorrectly to the fields produced by its model dynamics. This reduction in moisture flux occurs earlier in the forecast, which is indicative of it being a cause of the reduction in precipitation, but of course further investigation is required to confirm this.

The reduction in precipitation with forecast lead time seems to be strongly linked to an increase in moisture flux leaving the region to its east side that, in turn, is associated with anticyclonic flow to the northeast of India being replaced by purely westerly flow. This suggests that an inability to simulate low-pressure systems may be an important factor in the low-precipitation bias (it is also the case that an inability to simulate developing low-pressure systems moving into India from the east would be associated with a net increase in the westerly flow out of the region). The importance of low-pressure systems to the low-precipitation bias has previously been suggested by Levine and Martin (2018), and this could also be tested by tracking low-pressure systems for different BSISO phases in forecasts and observations/reanalyses (or for different forecast lead times), for example by using methods described by Hunt and Fletcher (2019).

The general flow entering the region from the west is also shown to decrease strongly, particularly from approximately day 3. This delayed reduction is consistent with the findings of Bush et al. (2015), who linked the low-precipitation bias over India with a high-precipitation bias over the Equatorial Indian Ocean, and found that changing the entrainment parameter over the Equatorial Indian Ocean could lead to improvements in the bias over India. It is possible that this bias dipole is exacerbated by a southward ITCZ bias in the UM. Kar et al. (2019) also found a reduction in flow from the west leading to reduced precipitation from 4 days in weather forecasts; this was also associated with an anticyclonic bias, but this time to the west of India and directly related to the reduction in westerly flow.

As well as looking at seasonal forecasts, it will be interesting to apply the analysis carried out in this study to longer simulations, to determine whether the same BSISO indices account for most, or even all, of the low-precipitation bias in these simulations, which would further confirm that the bias is due to similar mechanisms across time scales. Similarly, having ascertained that certain BSISO phases account for most of the bias, a useful next step would be to look at how other properties vary with BSISO index, to determine, for example, whether the UM is producing incorrect vertical profiles for the most problematic phases, or reacting incorrectly to realistic profiles.

Acknowledgments

The authors would like to thank Gill Martin, Prince Xavier, Melissa Brooks and John Marsham, for useful discussions related to this study. Richard Keane was supported by the Met Office Hadley Centre Climate Programme funded by BEIS and Defra and by the Weather and Climate Science for Service Partnership (WCSSP) India, a collaborative initiative between the Met Office, supported by the UK Governments Newton Fund, and the Indian Ministry of Earth Sciences (MoES). The work also benefitted from in-

sights gained during the INCOMPASS project (NERC NE/L013843/1). The source code for the models used in this study, UM and JULES, are available to use. To apply for a license for the UM go to `http://www.metoffice.gov.uk/research/collaboration/um-collaboration` and for permission to use JULES go to `https://jules.jchmr.org`. Data from the simulation and operational forecasts used in this study are archived at the Met Office and available for research use through the Centre for Environmental Data Analysis JASMIN platform (`http://www.jasmin.ac.uk/`); for details please contact `UM_collaboration@metoffice.gov.uk`. The 30-year climate simulation depicted in Figure S1 was carried out by Paul Earnshaw, and has identifier antia. Otherwise, the main operational forecasts were used in this study throughout (i.e., **not** the shorter updated forecasts, which are used to produce a more accurate analysis). Integrated Multi-satellitE Retrievals for GPM (IMERG) Final run data were obtained from `https:/arthurhou.pps.eosdis.nasa.gov` during the periods from 29 August 2019 to 19 September 2019 and from 17 February 2020 to 22 February 2020. Further observational precipitation data have been provided by GSMaP of the Japan Aerospace Exploration Agency, and were obtained from `hokusai.eorc.jaxa.jp/standard/v6/daily_Grev/00Z-23Z/$YYYY$MM` on 14–15 October 2020. GPCP Precipitation data were provided by the NOAA/OAR/ESRL PSL, Boulder, Colorado, USA, from their Web site at https://psl.noaa.gov/

References

Adler, R. F., Huffman, G. J., Chang, A., Ferraro, R., Xie, P.-P., Janowiak, J., ... Nelkin, E. (2003). The version-2 global precipitation climatology project (gpcp) monthly precipitation analysis (1979present). *Journal of Hydrometeorology*, *4*(6), 1147-1167. Retrieved from `https://doi.org/10.1175/1525-7541(2003)004<1147:TVGPCP>2.0.CO;2` doi: 10.1175/1525-7541(2003)004⟨1147:TVGPCP⟩2.0.CO;2

Almazroui, M., Saeed, S., Saeed, F., Islam, M. N., & Ismail, M. (2020). Projections of precipitation and temperature over the south asian countries in CMIP6. *Earth Syst. Environ.*, *4*, 297320. doi: 10.1007/s41748-020-00157-7

Bermous, I., & Steinle, P. (2015). Efficient performance of the Met Office Unified Model v8.2 on intel xeon partially used nodes. *Geoscientific Model Development*, *8*(3), 769–779. Retrieved from `https://www.geosci-model-dev.net/8/769/2015/` doi: 10.5194/gmd-8-769-2015

Bi, D., Dix, M., Marsland, S., O'Farrell, S., Rashid, H., Uotila, P., ... Puri, K. (2013). The ACCESS coupled model: description, control climate and evaluation. *Australian Meteorological and Oceanographic Journal*, *63*(1), 41-64. doi: 10.22499/2.6301.004

Brown, A., Milton, S., Cullen, M., Golding, B., Mitchell, J., & Shelly, A. (2012). Unified modeling and prediction of weather and climate: A 25-year journey. *Bulletin of the American Meteorological Society*, *93*(12), 1865-1877. Retrieved from `https://doi.org/10.1175/BAMS-D-12-00018.1` doi: 10.1175/BAMS-D-12-00018.1

Bush, S. J., Turner, A. G., Woolnough, S. J., Martin, G. M., & Klingaman, N. P. (2015). The effect of increased convective entrainment on asian monsoon biases in the MetUM general circulation model. *Quarterly Journal of the Royal Meteorological Society*, *141*(686), 311–326. Retrieved from `http://dx.doi.org/10.1002/qj.2371` doi: 10.1002/qj.2371

Goswami, B. N., & Xavier, P. K. (2003). Potential predictability and extended range prediction of indian summer monsoon breaks. *Geophysical Research Letters*, *30*(18). Retrieved from `https://agupubs.onlinelibrary.wiley.com/doi/abs/10.1029/2003GL017810` doi: 10.1029/2003GL017810

Gusain, A., Ghosh, S., & Karmakar, S. (2020). Added value of cmip6 over cmip5 models in simulating indian summer monsoon rainfall. *Atmospheric Research*, *232*, 104680. Retrieved from `http://www.sciencedirect.com/`

science/article/pii/S0169809519307665 doi: https://doi.org/10.1016/j.atmosres.2019.104680

Haywood, J. M., Jones, A., Dunstone, N., Milton, S., Vellinga, M., Bodas-Salcedo, A., ... Stephens, G. (2016). The impact of equilibrating hemispheric albedos on tropical performance in the hadgem2-es coupled climate model. *Geophysical Research Letters*, *43*(1), 395-403. Retrieved from https://agupubs.onlinelibrary.wiley.com/doi/abs/10.1002/2015GL066903 doi: 10.1002/2015GL066903

Huffman, G., Stocker, E., Bolvin, D., Nelkin, E., & Tan, J. (2019). *GPM IMERG Final precipitation L3 half hourly 0.1 degree x 0.1 degree V06*. Greenbelt, MD, Goddard Earth Sciences Data and Information Services Center (GES DISC). (Accessed: August 2019 – February 2020) doi: 10.5067/GPM/IMERG/3B-HH/06

Hunt, K., & Fletcher, J. (2019). The relationship between Indian monsoon rainfall and low-pressure systems. *Clim. Dyn.*, *53*, 1859-1871. doi: https://doi.org/10.1007/s00382-019-04744-x

Kar, S. C., Joshi, S., & Shrivastava, S. (2019). Dynamical characteristics of forecast errors in the NCMRWF unified model (NCUM). *Climate Dynamics*, *52*, 49955012. doi: 10.1007/s00382-018-4428-4

Keane, R. J., Williams, K. D., Stirling, A. J., Martin, G. M., Birch, C. E., & Parker, D. J. (2019). Fast biases in monsoon rainfall over southern and central India in the Met Office Unified Model. *Journal of Climate*, *32*(19), 6385-6402. doi: 10.1175/JCLI-D-18-0650.1

Kikuchi, K., Wang, B., & Kajikawa, Y. (2012). Bimodal representation of the tropical intraseasonal oscillation. *Climate Dyn.*, *38*, 1989-2000. doi: 10.1007/s00382-011-1159-1

Krishnamurthy, V., & Shukla, J. (2000, 12). Intraseasonal and Interannual Variability of Rainfall over India. *Journal of Climate*, *13*(24), 4366-4377. Retrieved from https://doi.org/10.1175/1520-0442(2000)013<0001:IAIVOR>2.0.CO;2 doi: 10.1175/1520-0442(2000)013⟨0001:IAIVOR⟩2.0.CO;2

Kubota, T., Aonashi, K., Ushio, T., Shige, S., Takayabu, Y. N., Kachi, M., ... Oki, R. (2020). Global satellite mapping of precipitation (gsmap) products in the gpm era. In V. Levizzani, C. Kidd, D. B. Kirschbaum, C. D. Kummerow, K. Nakamura, & F. J. Turk (Eds.), *Satellite precipitation measurement: Volume 1* (pp. 355–373). Cham: Springer International Publishing. Retrieved from https://doi.org/10.1007/978-3-030-24568-9_20 doi: 10.1007/978-3-030-24568-9_20

Levine, R. C., & Martin, G. M. (2018). On the climate model simulation of Indian monsoon low pressure systems and the effect of remote disturbances and systematic biases. *Climate Dynamics*. Retrieved from https://doi.org/10.1007/s00382-017-3900-x doi: 10.1007/s00382-017-3900-x

Martin, G. M., & Levine, R. C. (2012). The influence of dynamic vegetation on the present-day simulation and future projections of the south asian summer monsoon in the hadgem2 family. *Earth System Dynamics*, *3*(2), 245–261. Retrieved from https://www.earth-syst-dynam.net/3/245/2012/ doi: 10.5194/esd-3-245-2012

Noh, Y.-C., Sohn, B.-J., Kim, Y., Joo, S., & Bell, W. (2016). Evaluation of temperature and humidity profiles of Unified Model and ECMWF analyses using gruan radiosonde observations. *Atmosphere*, *7*(7). Retrieved from https://www.mdpi.com/2073-4433/7/7/94 doi: 10.3390/atmos7070094

Pathak, R., Sahany, S., Mishra, S., & Dash, S. K. (2019). Precipitation biases in CMIP5 models over the South Asian region. *Sci. Rep.*, *9*, 9589. doi: 10.1038/s41598-019-45907-4

Sharma, K., Ashrit, R., Ebert, E., Mitra, A., Bhatla, R., Iyengar, G., & Rajagopal, E. N. (2019).

J. Earth Syst. Sci., *128*(4). doi: https://doi.org/10.1007/s12040-018-1023-3

Sperber, K. R., Annamalai, H., Kang, I.-S., Kitoh, A., Moise, A., Turner, A., ... Zhou, T. (2013, Nov 01). The asian summer monsoon: an intercomparison of cmip5 vs. cmip3 simulations of the late 20th century. *Climate Dynamics*, *41*(9), 2711–2744. Retrieved from https://doi.org/10.1007/s00382-012-1607-6 doi: 10.1007/s00382-012-1607-6

Walters, D., Baran, A. J., Boutle, I., Brooks, M., Earnshaw, P., Edwards, J., ... Zerroukat, M. (2019). The Met Office Unified Model Global Atmosphere 7.0/7.1 and JULES Global Land 7.0 configurations. *Geoscientific Model Development*, *12*(5), 1909–1963. Retrieved from https://www.geosci-model-dev.net/12/1909/2019/ doi: 10.5194/gmd-12-1909-2019

Walters, D., Boutle, I., Brooks, M., Melvin, T., Stratton, R., Vosper, S., ... Xavier, P. (2017). The Met Office Unified Model Global Atmosphere 6.0/6.1 and JULES Global Land 6.0/6.1 configurations. *Geoscientific Model Development*, *10*(4), 1487–1520. Retrieved from https://www.geosci-model-dev.net/10/1487/2017/ doi: 10.5194/gmd-10-1487-2017

Wang, B., Jin, C., & Liu, J. (2020, 06). Understanding Future Change of Global Monsoons Projected by CMIP6 Models. *Journal of Climate*, *33*(15), 6471-6489. Retrieved from https://doi.org/10.1175/JCLI-D-19-0993.1 doi: 10.1175/JCLI-D-19-0993.1

Wang, B., & Xie, X. (1997). A model for the boreal summer intraseasonal oscillation. *J. Atmos. Sci.*, *54*, 72-86.

Webster, P., Magana, V., Palmer, T., Shukla, J., Tomas, R., Yanai, M., & Yasunari, T. (1998). Monsoons: processes, predictability, and theprospects for prediction. *J. Geophys. Res.*, *103*, 1445114510.

Wheeler, M., & Hendon, H. (2004). An all-season real-time multivariate MJO index: Development of an index for monitoring and prediction. *Mon. Wea. Rev.*, *132*, 19171932.

Willetts, P. D., Marsham, J. H., Birch, C. E., Parker, D. J., Webster, S., & Petch, J. (2017). Moist convection and its upscale effects in simulations of the Indian monsoon with explicit and parametrized convection. *Quarterly Journal of the Royal Meteorological Society*, *143*(703), 1073–1085. Retrieved from http://dx.doi.org/10.1002/qj.2991 doi: 10.1002/qj.2991

Williams, K. D., Copsey, D., Blockley, E. W., Bodas-Salcedo, A., Calvert, D., Comer, R., ... Xavier, P. K. (2018). The Met Office Global Coupled Model 3.0 and 3.1 (GC3.0 and GC3.1) configurations. *Journal of Advances in Modeling Earth Systems*, *10*(2), 357-380. Retrieved from https://agupubs.onlinelibrary.wiley.com/doi/abs/10.1002/2017MS001115 doi: 10.1002/2017MS001115

Zhu, B., & Wang, B. (1993, 01). The 3060-Day Convection Seesaw between the Tropical Indian and Western Pacific Oceans. *Journal of the Atmospheric Sciences*, *50*(2), 184-199. Retrieved from https://doi.org/10.1175/1520-0469(1993)050<0184:TDCSBT>2.0.CO;2 doi: 10.1175/1520-0469(1993)050⟨0184:TDCSBT⟩2.0.CO;2